Supporting Information

Regulating Ni_2P electronic structure and morphology with cobalt: A one-step route to enhanced electrocatalytic urea oxidation and water splitting

Peng Zhang [a, +], Fozia Sultana [a, +], Tongtong Li [a, *], Xiaojun Qin [a], Meijie Shi [a], Tong Wei [a], Kaicheng Qian [a], Mingwu Tan [b, *], Zhixue Li[c], Jianming Bai[c,*], Renhong Li [a, *]

[a] National Engineering Lab for Textile Fiber Materials and Processing Technology, School of Materials Science & Engineering, Zhejiang Sci-Tech University, Hangzhou 310018, China

[b] Institute of Sustainability for Chemicals, Energy and Environment (ISCE2), Agency for Science, Technology and Research (A*STAR), 1 Pesek Road, Jurong Island, 627833, Singapore

[c] Huadian Heavy Industries Co. Ltd (HHI), Huadian Industrial Park, No. 6 East Road, Automobile Museum, Fengtai District, Beijing, 100160, China

[+] These authors contributed equally to this work.

[*] Corresponding author.

E-mail addresses: lirenhong@zstu.edu.cn (R. Li), baijm@chec.com.cn (J. Bai), tan_mingwu@isce2.a-star.edu.sg (M. Tan), yitaji@zstu.edu.cn (T. Li)

Characterizations

The samples underwent analysis to assess their morphology, phase characteristics, and elemental composition utilizing a scanning electron microscope (SEM, Zeiss Sigma 300), a transmission electron microscope (TEM, FEI Talos f200x), and wide-angle X-ray diffraction (XRD) patterns obtained from a Bruker D8 diffractometer equipped with Cu Ka radiation. The surface chemical states of the elements in the catalysts were determined through X-ray photoelectron spectroscopy (XPS, Thermos Scientific ESCALAB 250Xi), with all XPS spectra calibrated against the C 1s spectrum at a binding energy of 284.8 eV.

Electrochemical measurements

The electrochemical experiments were conducted in a conventional three-electrode configuration with a CHI750E electrochemical workstation. A platinum wire was employed as the counter electrode, whereas a mercury/mercury oxide (Hg/HgO) reference electrode in a 3M KCl solution was utilized for reference purposes. All the measured potentials are transformed into a reversible hydrogen electrode (RHE) system using the following equation: $E_{RHE}= E_{Hg/HgO} + 0.059$ PH + 0.098 V. All the working electrodes underwent electrochemical activation through the execution of 50 cycles of cyclic voltammetry (CV) within a potential range of −1.5 to 0.8 V (vs. RHE), utilizing a scan rate of 20 mV s^{-1} in a 1 M KOH solution, both with and without the addition of 0.5 M urea. The linear sweep voltammetry (LSV) technique for both UOR and OER was measured at a scan rate of 2 mV s^{-1} in a 1.0 M KOH solution, with and without the incorporation of 0.5 M urea. Tafel slopes are calculated using the Tafel equation: $\eta = a$

+b * log j， where η represents the overpotential, a refers to the intercept associated with the exchange current density (j), b denotes the Tafel slope, and j indicated the current density.

The electrochemically active surface areas (ECSA) of the electrocatalysts were determined using the following equation:

$$ECSA = \frac{C_{dl}}{C_s}$$

C_{dl} represents the electrochemical double-layer capacitance, which is determined from the series of CV obtained in the non-Faradaic region of 1.0 to 1.1 V (vs. RHE), using different scan rate of 5, 10, 20, 30, 40, 50 60 and 70 mV s^{-1}. Electrochemical impedance spectroscopy (EIS) tests are collected by applying an alternating current (AC) potential amplitude of 10 mV with frequency ranging from 10^{-2} Hz to 10^{8} Hz at 1.45 V (vs. RHE). Additional, chronopotentiometry was carried out to monitor the operation durability of electrocatalysts.

DFT calculation

All the calculations were performed in the framework of the density functional theory with the projector augmented plane-wave method, as implemented in the VASP[1]. The generalized gradient approximation proposed by Perdew, Burke, and Ernzerhof[2] screened hybrid density functional were selected for the exchange-correlation potential[3]. The van der Waals interactions was characterized utilizing the DFT-D3 methodology[4]. A plane wave cut-off energy of 400 eV was established. The energy convergence criterion for the iterative resolution of the Kohn-Sham equations was set at 10^{-4} eV. To prevent spurious interactions between periodic images, a vacuum layer measuring 20 Å was incorporated perpendicular to the sheet. The integration over the Brillouin zone was conducted using a 2 x 2 x 1 K-mesh. All structures underwent relaxation until the residual forces acting on the atoms were reduced to below 10^{-5} eV/Å.

The adsorption energy was defined as:

$$E_{ads} = E_{\frac{A}{M}} - E_A - E_M$$

where $E_{\frac{A}{M}}$, E_A, and E_{M} are the total energies of the molecule adsorbed on the surface[5], an isolated molecule, and the surface, respectively.

The oxidation of urea into CO_2 and N_2 occurs in the following consecutive elementary steps:

$$CO(NH_2)_{2(aq)} \rightarrow CO(NH_2)_2{}^{*} \qquad (R_1)$$

$$CO(NH_2)_2{}^{*} + OH^- \rightarrow CO(NH_2NH)^{*} + H_2O + e^- \qquad (R_2)$$

$$CO(NH_2NH)^{*} + OH^- \rightarrow CO(NH_2N)^{*} + H_2O + e^- \qquad (R_3)$$

$$CO(NH_2N)^{*} + OH^- \rightarrow CO(NHN)^{*} + H_2O + e^- \qquad (R_4)$$

$$CO(NHN)^{*} + OH^- \rightarrow CON_2{}^{*} + H_2O + e^- \qquad (R_5)$$

$$CON_2{}^{*} + OH^- \rightarrow CO^{*} + N_{2(g)} \qquad (R_6)$$

$$CO^{*} + OH^- \rightarrow COOH^{*} + e^- \qquad (R_7)$$

$$COOH^{*} + OH^- \rightarrow CO_{2(g)} + H_2O + e^- \qquad (R_8)$$

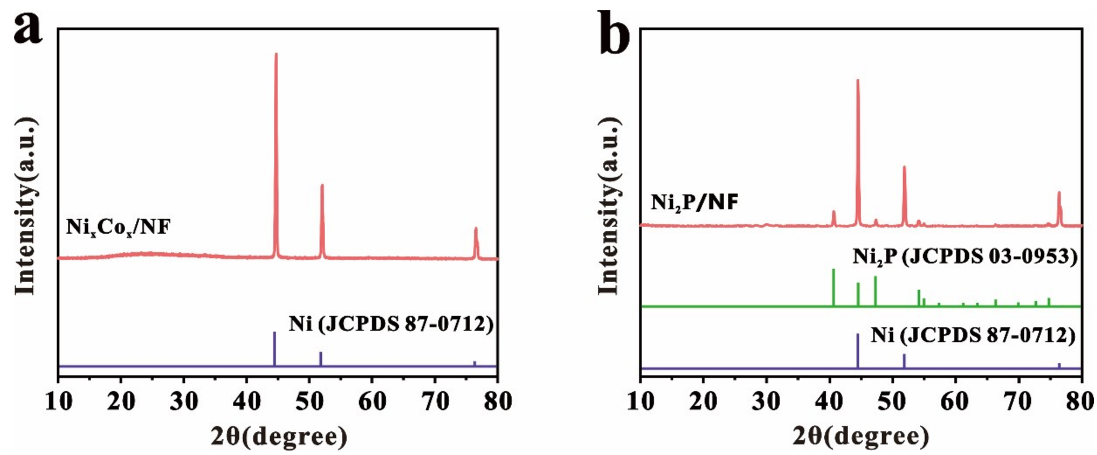

Figure S1. XRD images of (a) Ni_xCo_x/NF and (b) Ni_2P/NF.

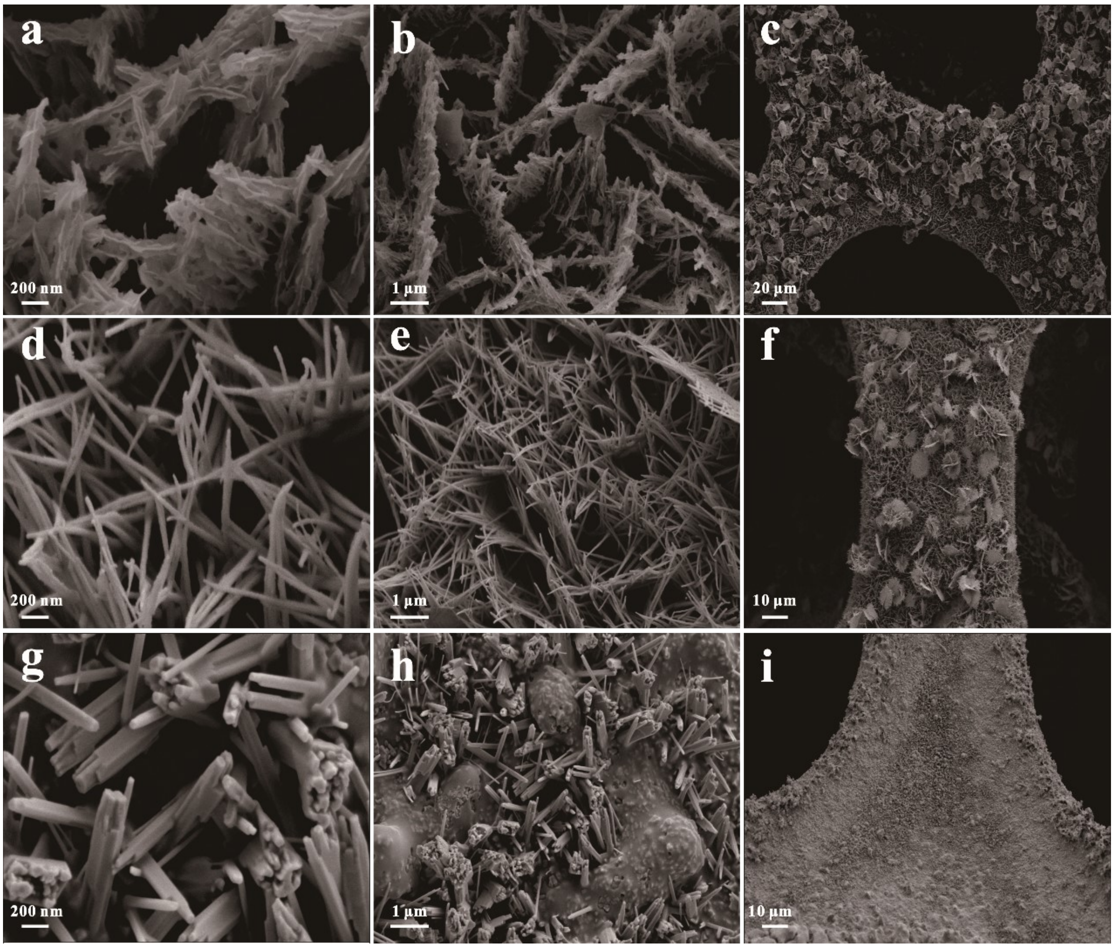

Figure S2. SEM images of (a-c) Ni_xCo_x/NF, (d-f) Ni_2P/NiCoP/NF, and (g-i) Ni_2P/NF.

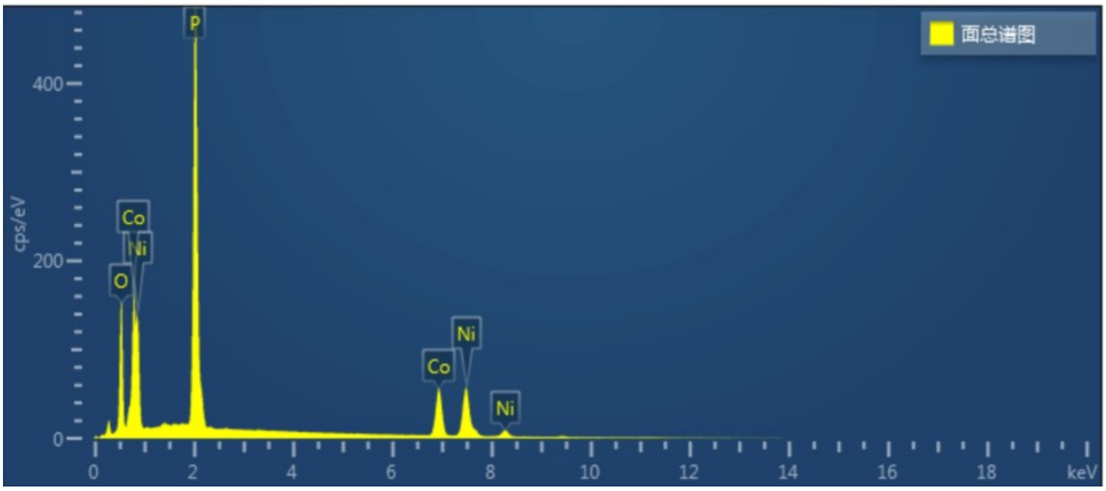

Figure S3. EDX spectra of Ni_2P/NiCoP/NF.

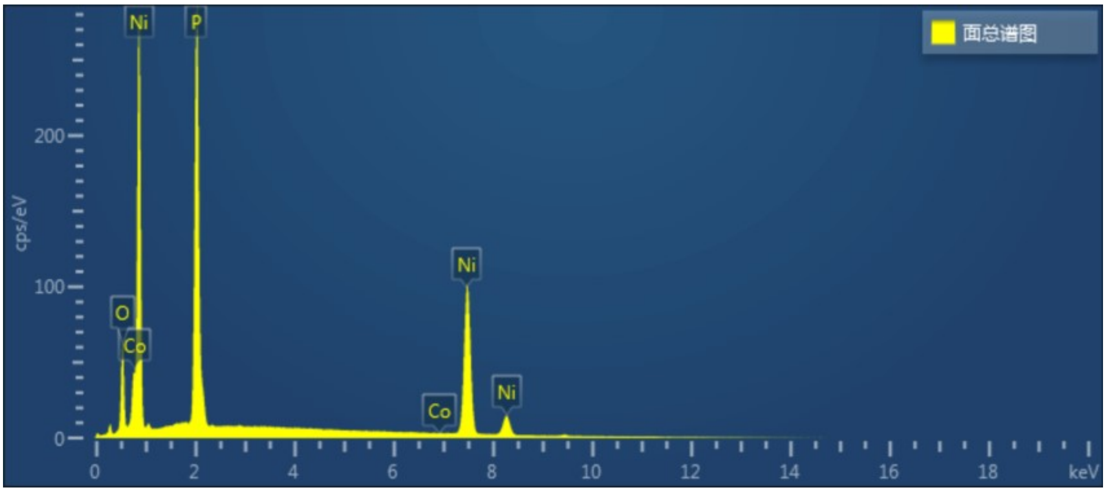

Figure S4. EDX spectra of Ni_2P/NF.

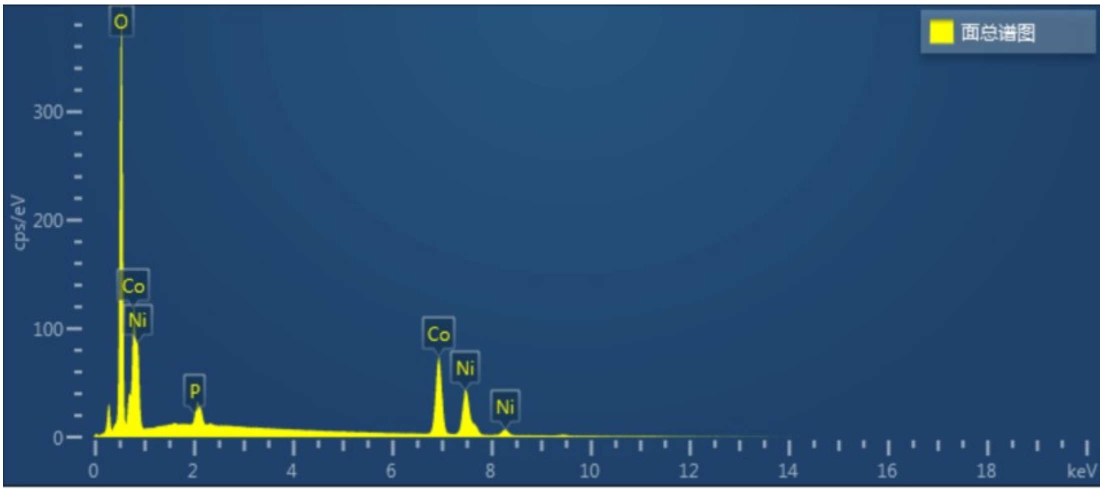

Figure S5. EDX spectra of Ni_xCo_x/NF.

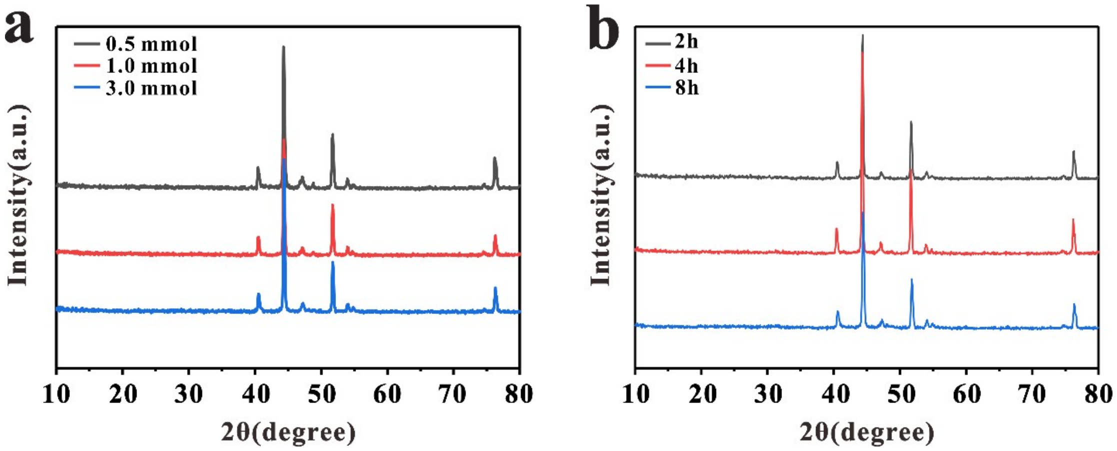

Figure S6. (a) XRD images of Ni_2P/NiCoP/NF with different Co salts content and (b) different reaction time with the same reaction temperature.

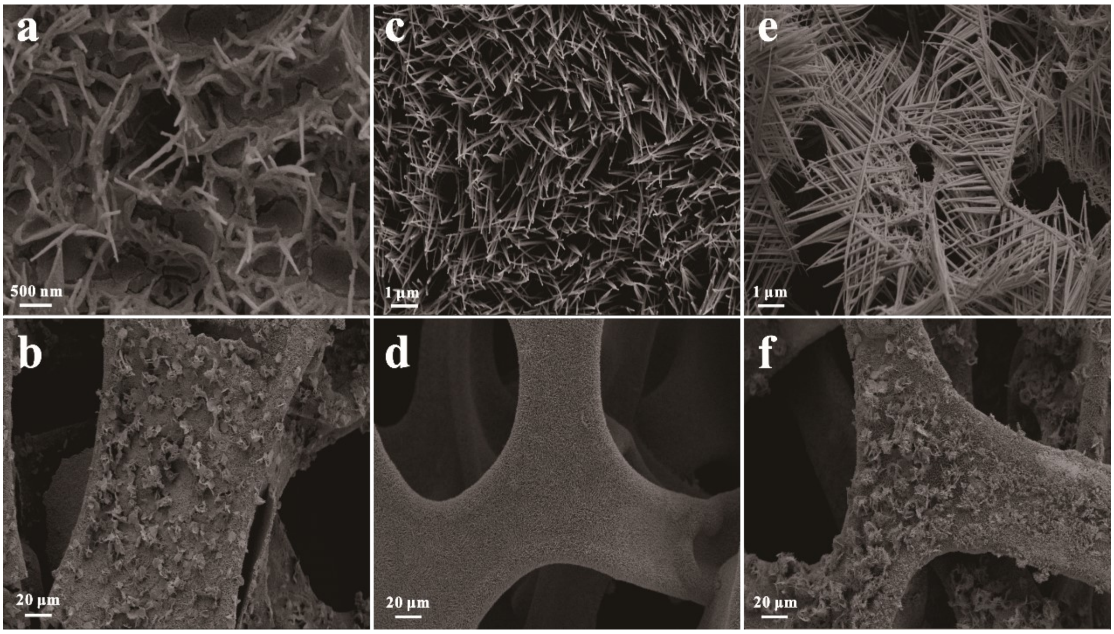

Figure S7. SEM images of Ni_2P/NiCoP/NF with different Co salts content under the same other conditions (0.5 mmol (a-b), 1 mmol (c-d), and 3 mmol (e-f)).

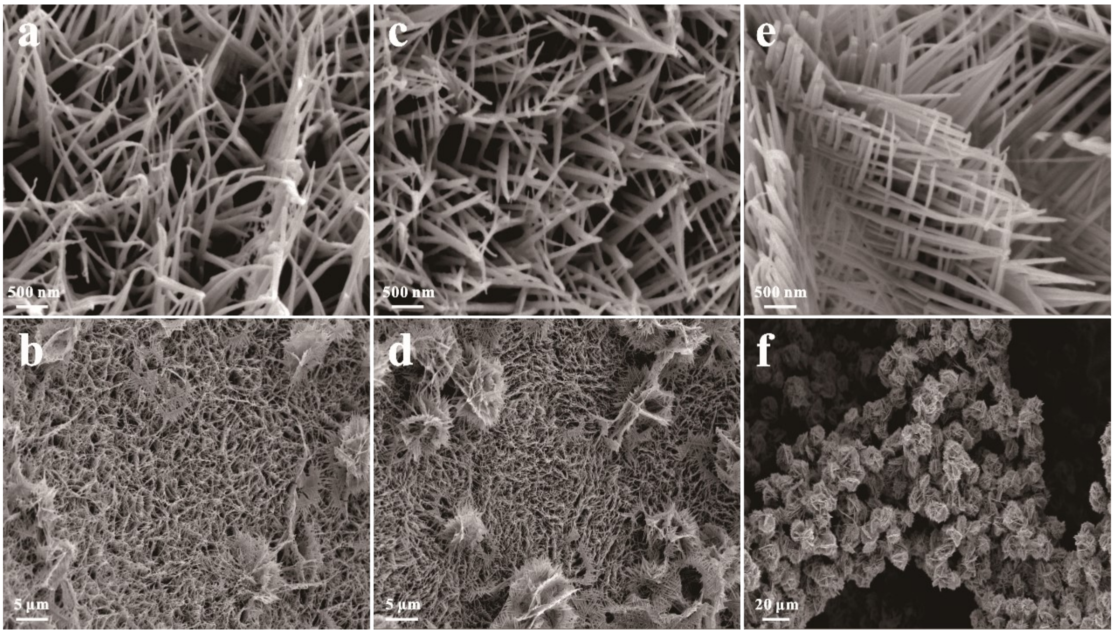

Figure S8. Microscopy measurements of the Ni_2P/NiCoP/NF at different reaction time with the same reaction temperature of 120 ˚C. SEM images of Ni_2P/NiCoP/NF prepared at different reaction time (2 h (a-b), 4 h (c-d), and 8 h (e-f)).

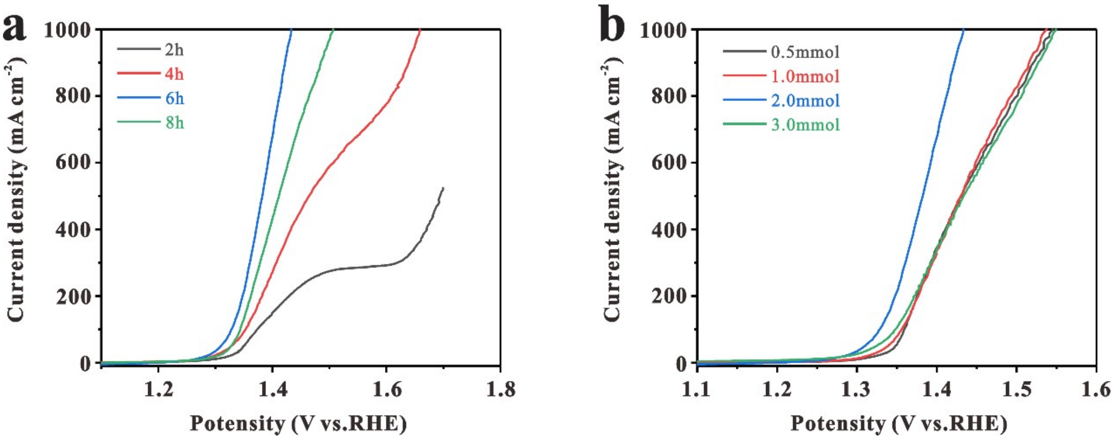

Figure S9. Polarization curves of Ni_2P/NiCoP/NF with (a) different hydrothermal temperature and (b) different Co salts.

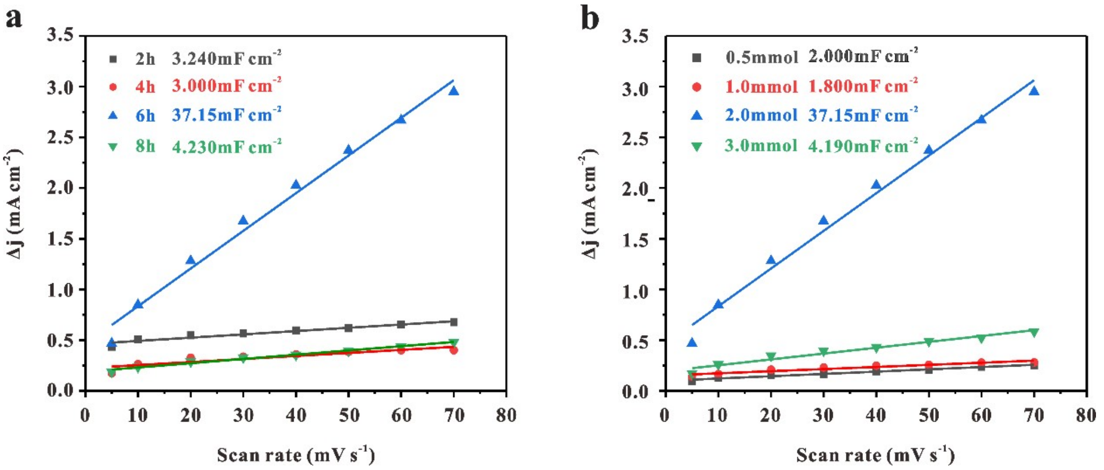

Figure S10. Double-layer capacitances of Ni_2P/NiCoP/NF with (a) different hydrothermal temperature and (b) different Co salts.

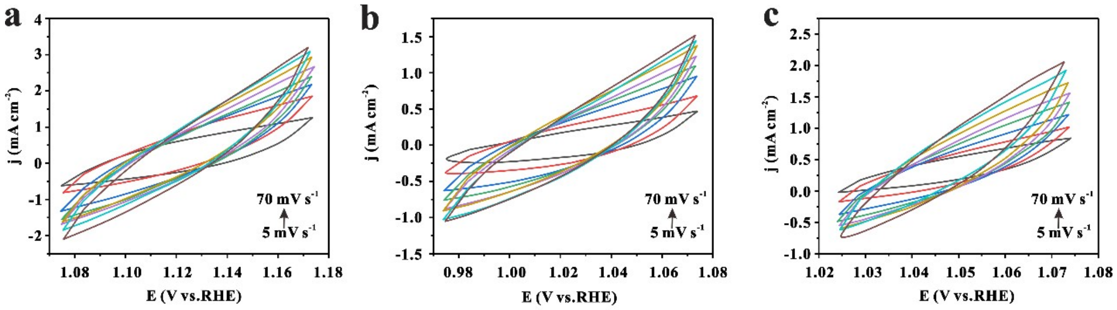

Figure S11. The CVs of Ni_2P/NiCoP/NF with different hydrothermal time ((a) 2 h, (b) 4 h, and (c) 8 h).

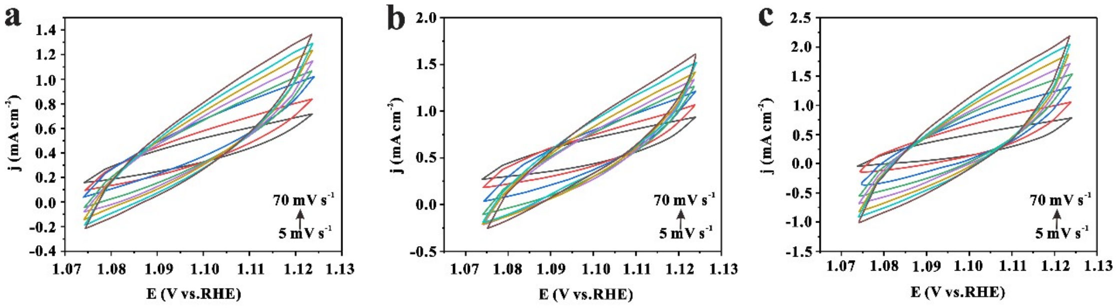

Figure S12. The CVs of Ni_2P/NiCoP/NF with different Co salts ((a) 0.5 mmol, (b) 1 mmol, and (c) 3 mmol).

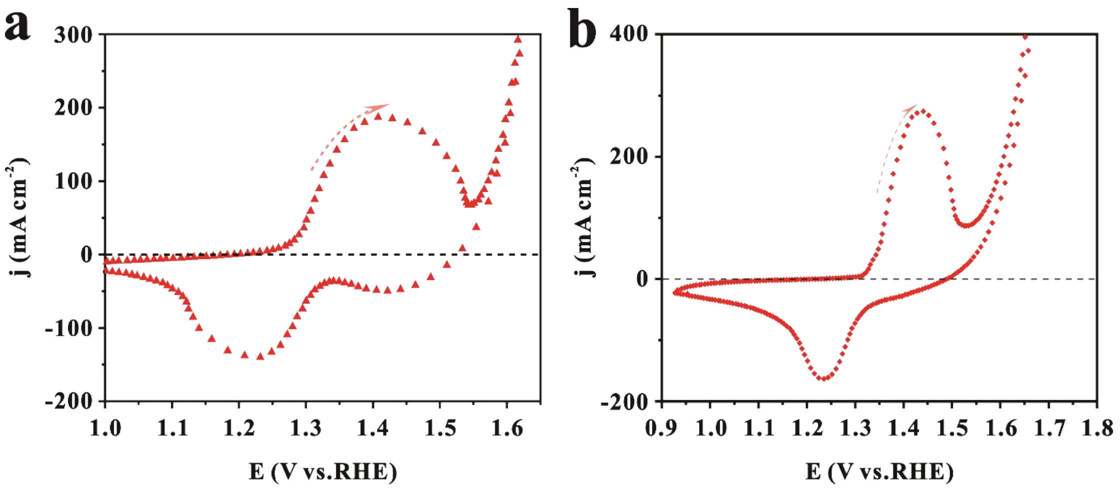

Figure S13. The CV curve of (a) Ni_2P/NiCoP/NF and (b) Ni_2P/NF in 1.0 M KOH.

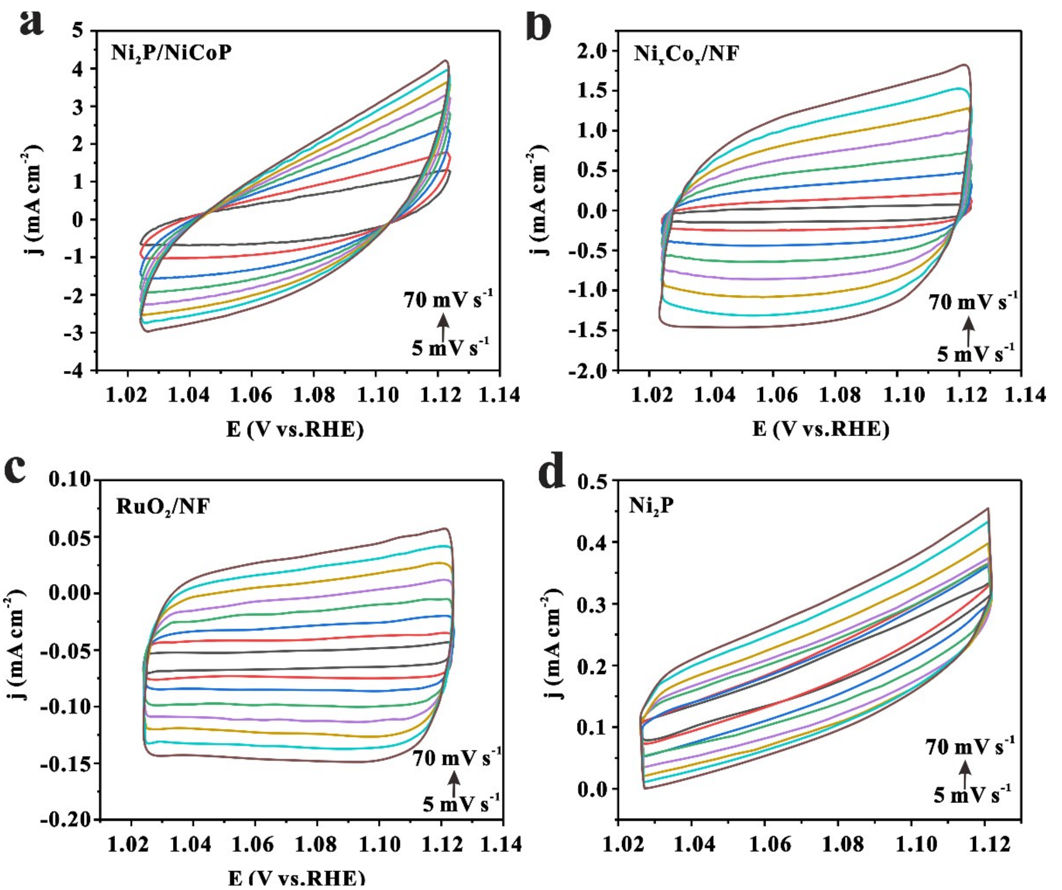

Figure S14.The CVs of (a) Ni_2P/NiCoP/NF, (b) Ni_xCo_x/NF, (c) RuO_2/NF, and Ni_2P/NF in 1.0 M KOH containing 0.5 M urea.

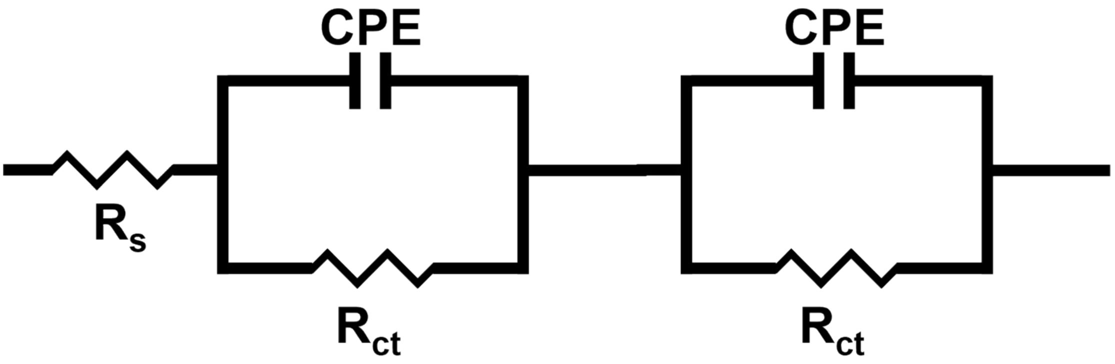

Figure S15. Electrical equivalent circuit model used for analyzing the interfacial charge transfer. The R_s represents the solution resistance, the R_{ct} and CPE in parallel represents the charge transfer resistance and double layer capacitance at the electrode interface.

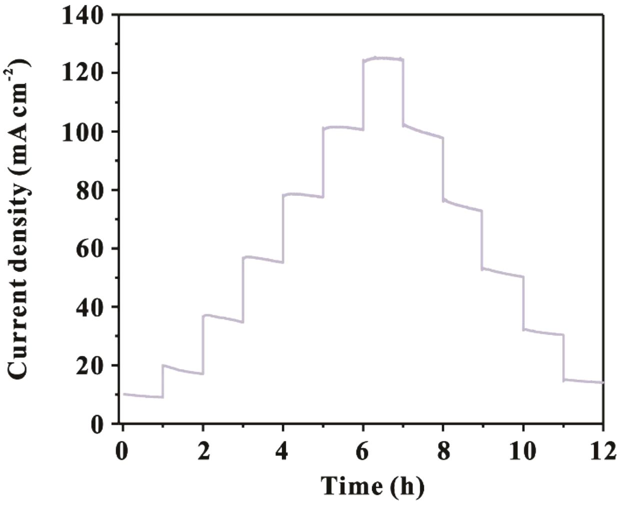

Figure S16. The multistep chronopotentiometry test at different current densities.

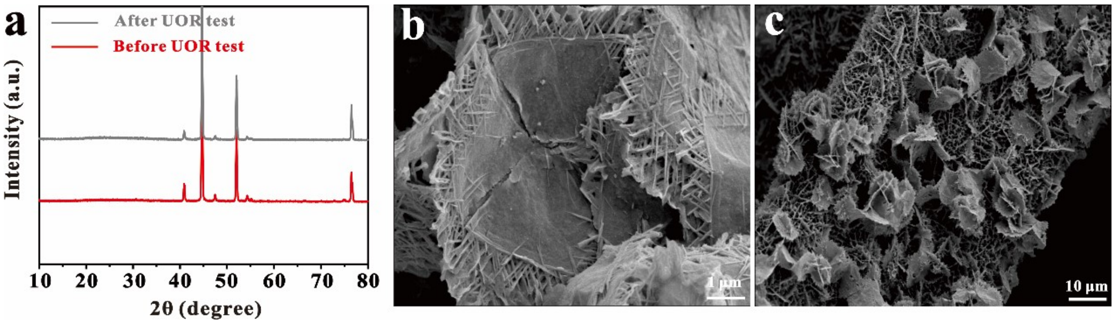

Figure S17. (a) The XRD patterns of Ni_2P/NiCoP/NF before and after UOR stability test, (b-c) the SEM images of Ni_2P/NiCoP/NF after UOR stability test.

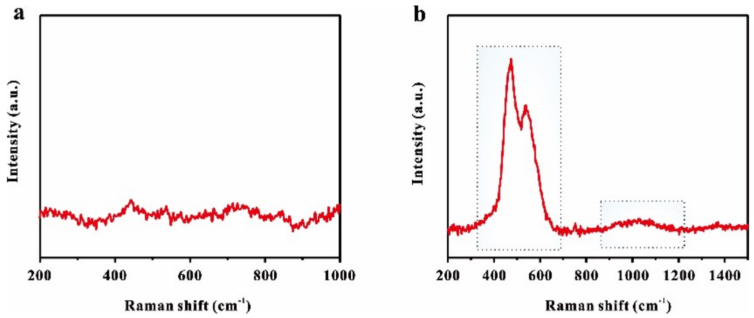

Figure S18. Raman spectra of (a) Ni_2P/NiCoP/NF before and (b) after UOR test.

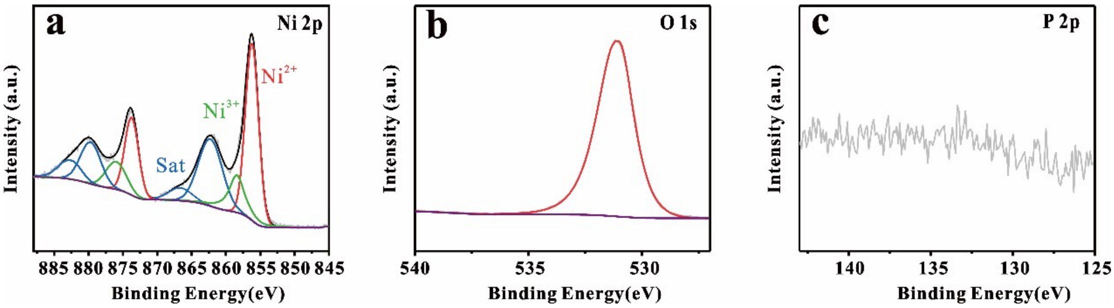

Figure S19. The high-resolution (a) Ni 2p, (b) O 1s, and (P 2p) XPS specter of Ni_2P/NF after the UOR stability test.

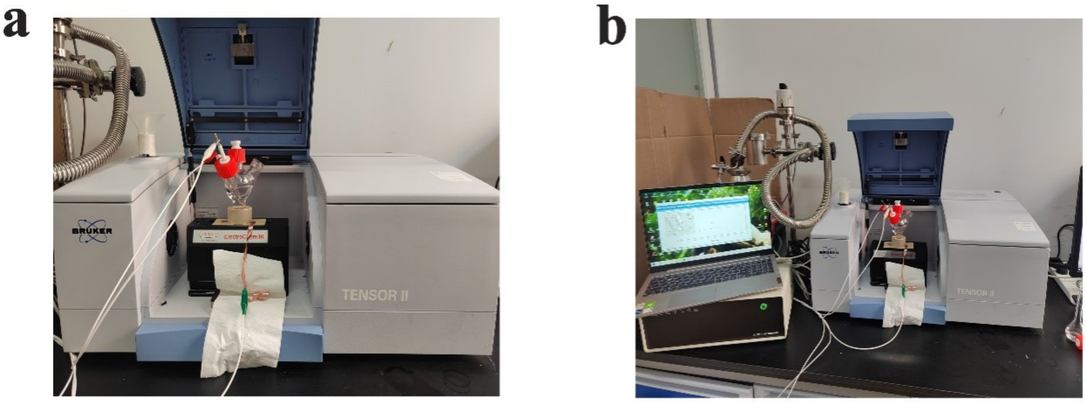

Figure S20. (a-b) Photos depicting the setup of in situ ATR-SEIRAS experiments, Mechanism of Ni_2P/NiCoP/NF electrocatalytic urea oxidation.

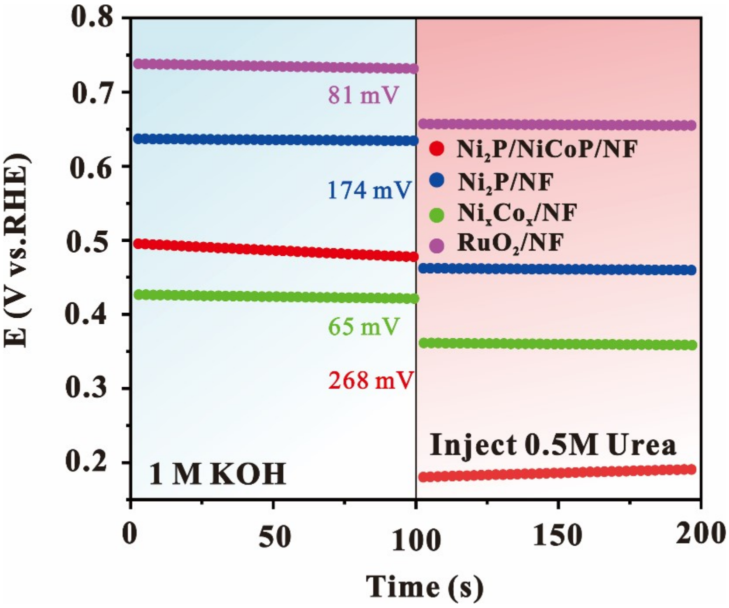

Figure S21. OCP curves before and after injection of 0.5 M Urea

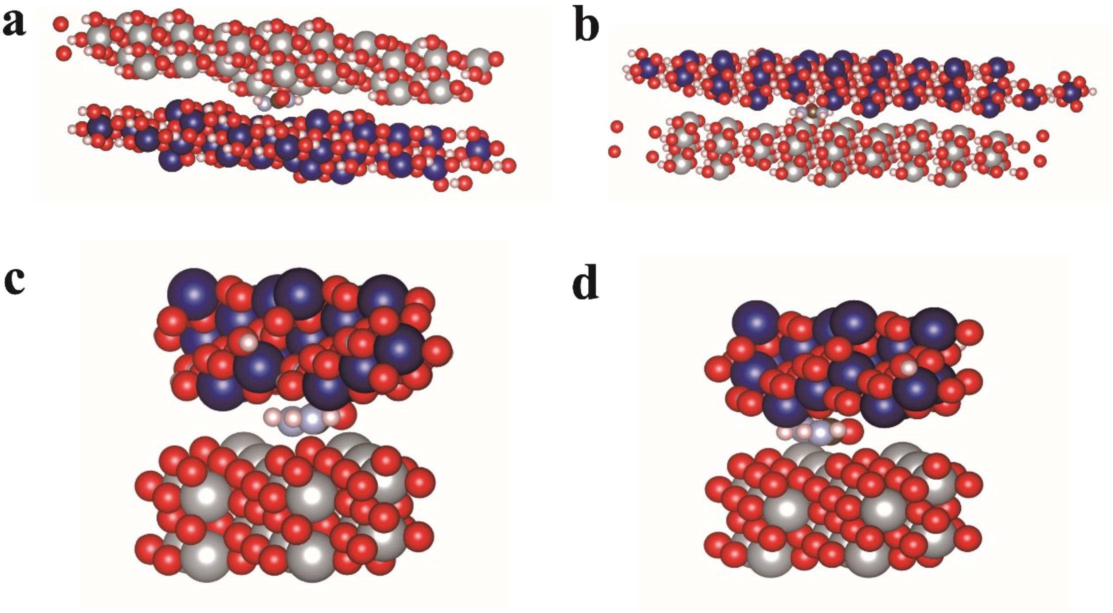

Figure S22. The urea adsorption models of (a) NiOOH-CoOOH/NF (Ni-O), (b) NiOOH-CoOOH/NF (Ni-N), (c) NiOOH-CoOOH/NF (Co-O), (d) NiOOH-CoOOH/NF (Co-N).

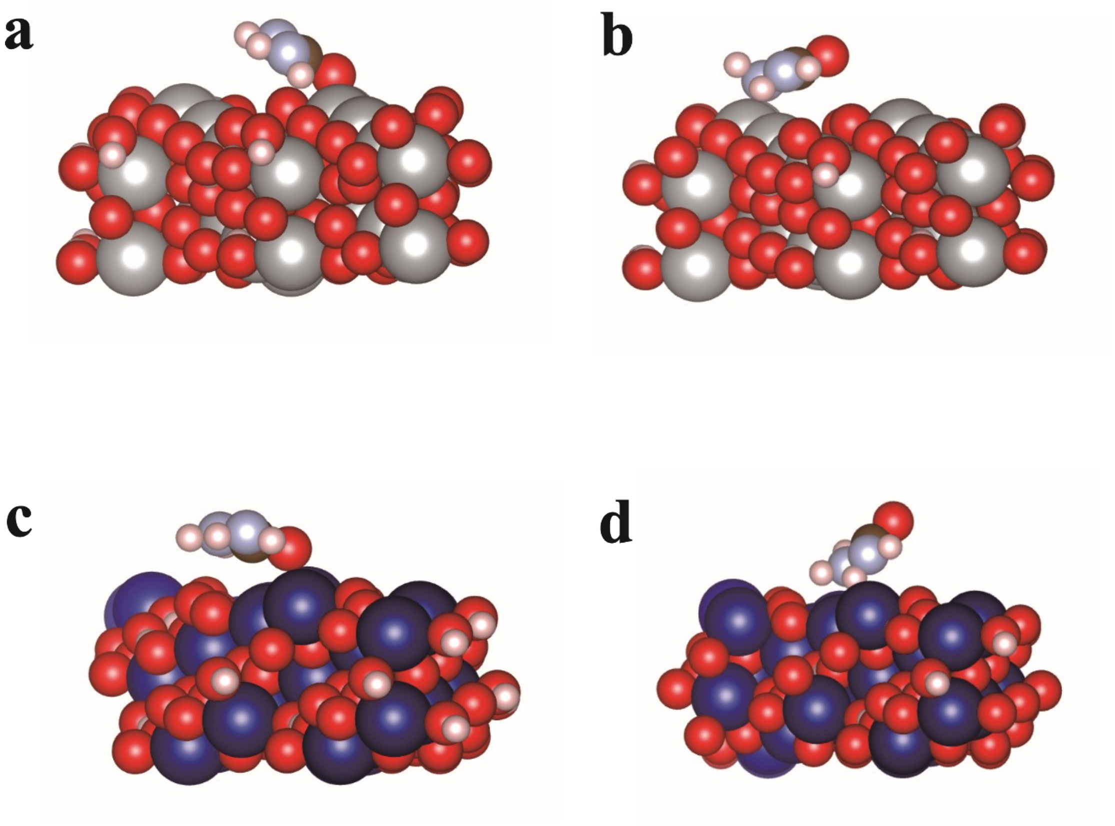

Figure S23. The urea adsorption models of (a) NiOOH/NF (Ni-O), (b) NiOOH/NF (Ni-N), (c) CoOOH/NF (Co-O), (d) CoOOH/NF (Co-N).

Table S1. EDX data of Ni_2P/NiCoP/NF

Element	**Atomic (%)**
Ni	21.1
Co	16.36
P	33.7

Table S2. EDX data of Ni_2P/NF

Element	**Atomic (%)**
Ni	45.93
P	25.03

Table S3. EDX data of Ni_xCo_x/NF

Element	**Atomic (%)**
Ni	11.31
Co	15.23
O	73.45

Table S4. Comparison of electrocatalytic organic oxidation performance of Ni_2P/NiCoP/NF with other reported catalysts.

Catalysts	**Urea Concentration**[1]	**$E_{j=100}$ (V vs. RHE)**	**Ref.**
Ni_2P/NiCoP/NF	0.5M	1.31	This work
P-$NiMoO_4$	0.33M	1.35	[6]
Ni_3S_2@Ni_3P	0.33	1.36	[7]
c-$CoNiP_{x/}$a-P-MnO_y	0.5M	1.35	[8]
A-NF	0.33M	1.44	[9]
$NiMoO_4$-300/NF	0.5M	1.38	[10]
Co–Ni–S@NF	0.33M	1.35	[11]
W-NT@NF	0.33M	1.43	[12]
$Ni_{0.8}Co_{0.2}$ DHs	0.33M	1.35	[13]
[Fe_2P/Co_2P]@Mo_2S_3/NF	0.5M	1.36	[14]
$NiMoO_4 \cdot H_2O$	0.33M	1.34	[15]
aFe-NiB	0.5M	1.34	[16]
S-Co_2P@Ni_2P	0.5M	1.36	[17]
Ni/MNO-10	0.5M	1.43	[18]
P-$CoNi_2S_4$	0.5M	1.36	[19]

[1] The electrolyte was 1 M KOH with different concentrations of urea.

~ The value was obtained from the LSV curves in the corresponding paper.

References

1. G. Kresse and D. Joubert, *Phy. Rev. B*, 1999, **59**, 1758-1775.
2. J. Heyd, G. E. Scuseria and M. Ernzerhof, *J. Chem. Phys.*, 2003, **118**, 8207-8215.
3. J. P. Perdew, K. Burke and M. Ernzerhof, *Phys. Rev. Lett.*, 1996, **77**, 3865-3868.
4. S. Grimme, J. Antony, S. Ehrlich and H. Krieg, *J. Chem. Phys.*, 2010, **132**.
5. T. Li, Y. Yu and M. Pei, *J.Phys. Chem. C*, 2023, **127**, 6271-6279.
6. Z.-H. Yin, Y. Huang, L.-W. Jiang, C. Meng, Y.-Z. Wu, H. Liu and J.-J. Wang, *Small*, 2023, **4**.
7. X. Guo, L. Qiu, M. Li, F. Tian, X. Ren, S. Jie, S. Geng, G. Han, Y. Huang, Y. Song, W. Yang and Y. Yu, *Chem. Eng. J.*, 2024, **483**.
8. L. Qiao, A. Zhu, D. Liu, J. Feng, Y. Chen, M. Chen, P. Zhou, L. Yin, R. Wu, K. W. Ng and H. Pan, *Chem. Eng. J.*, 2023, **454**.
9. Z. Tu, X. Liu, D. Xiong, J. Wang, S. Gong, C. Xu, D. Wu and Z. Chen, *Chem. Eng. J.*, 2023, **475**.
10. C. Chen, S. He, K. Dastafkan, Z. Zou, Q. Wang and C. Zhao, *Chinese Journal of Catalysis*, 2022, **43**, 1267-1276.
11. Z. Xu, Q. Chen, Q. Chen, P. Wang, J. Wang, C. Guo, X. Qiu, X. Han and J. Hao, *J. Mater. Chem. A*, 2022, **10**, 24137-24146.
12. M. Liu, W. Zou, S. Qiu, N. Su, J. Cong and L. Hou, *Adv. Funct. Mater.*, 2023, **34**.
13. X. Yang, H. Zhang, B. Yu, Y. Liu, W. Xu and Z. Wu, *Energr technol*, 2022, **10**, 2101010.
14. L. Wang, W. He, D. Yin, Y. Xie, H. Zhang, Q. Ma, W. Yu, Y. Yang and X. Dong, *Chem. Eng. J.,* 2023, **462**.
15. Y. Zhu, C. Liu, S. Cui, Z. Lu, J. Ye, Y. Wen, W. Shi, X. Huang, L. Xue, J. Bian, Y. Li, Y. Xu and B. Zhang, *Adv. Mater.*, 2023, **35**.
16. Z. Chen, R. Zheng, H. Zou, R. Wang, C. Huang, W. Dai, W. Wei, L. Duan, B.-J. Ni and H. Chen, *Chem. Eng. J.*, 2023, **465**.
17. W. Yuan, T. Jiang, X. Fang, Y. Fan, S. Qian, Y. Gao, N. Cheng, H. Xue and J. Tian, *Chem. Eng. J.*, 2022, **439**.
18. V. Maheskumar, A. Min, C. J. Moon, R. A. Senthil and M. Y. Choi, *Small*, 2023, **4**.
19. X. F. Lu, S. L. Zhang, W. L. Sim, S. Gao and X. W. D. Lou, *Angew. Chem. Int. Ed.*, 2021, **60**, 22885-22891.